ARTICLE

Temperature-Dependence of the Amide-I Frequency Map for Peptides and Proteins†

Chen Han, Jian-ping Wang*

Beijing National Laboratory for Molecular Sciences, State Key Laboratory of Molecular Reaction Dynamics, Institute of Chemistry, Chinese Academy of Sciences, Beijing 100190, China

(Dated: Received on July 28, 2011; Accepted on September 27, 2011)

In our recent work [Phys. Chem. Chem. Phys. **11**, 9149 (2009)], a molecular-mechanics force field-based amide-I vibration frequency map (MM-map) for peptides and proteins was constructed. In this work, the temperature dependence of the MM-map is examined based on high-temperature molecular dynamics simulations and infrared (IR) experiments. It is shown that the 298-K map works for up to 500-K molecular dynamics trajectories, which reasonably reproduces the 88 °C experimental IR results. Linear IR spectra are also simulated for two tripeptides containing natural and unnatural amino acid residues, and the results are in reasonable agreement with experiment. The results suggest the MM-map can be used to obtain the temperature-dependent amide-I local mode frequencies and their distributions for peptide oligomers, which is useful in particular for understanding the IR signatures of the thermally unfolded species.

Key words: Amide-I, Frequency map, Infrared spectrum, Molecular dynamics simulation

I. INTRODUCTION

The studies of backbone carbonyl stretching motion, *i.e.*, the amide-I mode, as a secondary structural marker of peptides and proteins, have been an intense subject in recent years [1−7]. Using this marker, time-resolved linear infrared (IR) and nonlinear IR methods, for example, two-dimensional IR (2D IR) [1], have been applied successfully to examine the structures and dynamics of peptides and proteins. Information details gained at the level of chemical bond allow one to get a microscopic picture of the ultrafast protein conformational dynamics, hydrogen-bonding dynamics, protein-solvent interaction, protein folding as well as protein aggregations.

Experimentally observed linear IR and 2D IR spectra of the amide-I band of a given polypeptide are in a normal mode picture, in which a collection of amide-I vibrators are coupled to one another. To fully understand these spectra, it is crucial to obtain a local mode picture of the amide-I band, where the amide-I vibrators are decoupled. In recent years, several electrostatic maps were established with the aid of quantum chemical computations and molecular dynamics (MD) simulations [8−16], through which the amide-I local mode frequencies are connected to the electrostatic potential or field on amide units, which is generated by peptide chain and solvent molecules. The applications of these frequency maps on linear IR and 2D IR spectral interpretations and simulations have been reported [9, 10, 17]. In our recent work, a molecular mechanics (MM) force field-based empirical electrostatic potential map (MM-map) for amide-I vibrations was developed mainly based on the MD simulations [11]. The instantaneous amide-I vibrational parameters (transition frequency and transition dipole) obtained at the level of MM force fields are converted to solution phase values by a four-site electrostatic potential scheme. In comparison with recently developed *ab initio* computation-based electrostatic potential or field maps mentioned above, our approach works reasonably. The transferability of the frequency maps has been tested in different solvents in several cases [11, 12]; however, none of the maps has been tested for temperature dependence.

In this work, we examined the temperature dependence of the MM-map, aiming to assess the local mode frequencies and their distributions associated with the thermally unfolded peptides and proteins. The local mode properties of the amide-I band were modeled using a specially designed monopeptide compound, N-methylacetamide (NMA, $CH_3CONHCH_3$, Fig.1). We firstly simulated the temperature-dependent amide-I IR spectra of NMA, then two unnatural tripeptides containing H-propargylglycine-OH (Pra), namely Ac-Pra-Pra-NH_2 (PPTP, Fig.1) and Ac-Pra-Ala-NH_2 (PATP), were used to test the temperature-dependence of the MM frequency map. For this, MD simulations at

†Part of the special issue for "the Chinese Chemical Society's 12th National Chemical Dynamics Symposium".

*Author to whom correspondence should be addressed. E-mail: jwang@iccas.ac.cn, Tel.: +86-10-62656806, FAX: +86-10-62563167

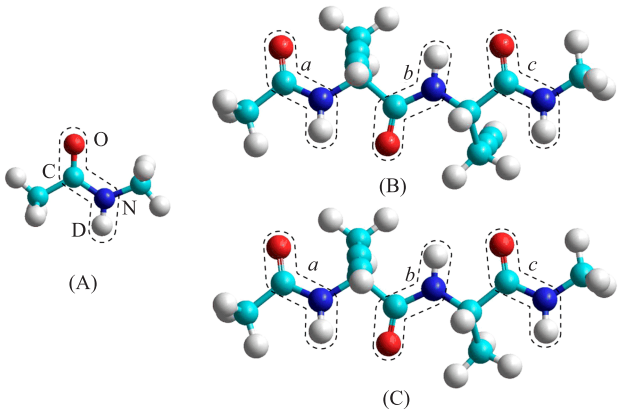

FIG. 1 Structures of NMA (A), PPTP (B), and PATP (C). Amide units are marked with dashed lines and are labeled *a*, *b*, and *c* in PPTP and PATP, starting from the acetyl end.

298 and 500 K were carried out for PPTP and PATP in explicit water environment. Linear IR spectra for these peptide oligomers in the amide-I region were simulated using the frequency time-correlation functions (TCFs) on the basis of the MM-map.

II. MATERIALS AND METHODS

A. Materials

NMA (99% purity) was purchased from Sigma-Aldrich. Fmoc-Pra-OH (95% purity) was purchased from Bachem for peptide synthesis. D_2O (99.9% purity) was purchased from Cambridge Isotope Laboratories. Two Pra-containing tripeptides of PPTP and PATP were synthesized by standard Fmoc protocol with 90% purity. NMA, PPTP, and PATP were lyophilized three times in D_2O for H/D exchange of the amide NH group.

B. Infrared spectroscopy

The IR spectra were measured using Nicolet 6700 FTIR spectrometer equipped with a liquid nitrogen-cooled mercury-cadmium-telluride detector. The concentrations for NMA, PPTP, and PATP in D_2O were 41.5, 54.0, and 45.8 mmol/L respectively. The IR spectra of NMA, PPTP and PATP were measured between 23 and 88 °C. The IR spectra were recorded with a spectral resolution of 1 cm^{-1}, averaged by 64 scans. All of the samples were placed in a home-made dual CaF_2 IR cell with a 100 μm Teflon spacer. The dual IR cell contained two 2-mm thick CaF_2 windows and shared the same Teflon spacer but had two independent sample compartments. The two compartments were used to contain peptide sample solution and D_2O only respectively. The dual cell was placed on a motorized translation stage so that the sample and reference spectra could be taken alternatively to diminish air moisture influence and increase signal-to-noise ratio. Dry air was used to purge the FTIR spectrometer and sample chamber during the spectral measurements.

C. MD simulations of PPTP and PATP

The classic MD simulations for NMA, PPTP, and PATP at room and high temperatures were performed using NAMD [18] with the CHARMM force fields [19] including the Φ-Ψ cross term (CMAP) correction [20]. The force field parameters of the −C≡CH group of Pra residue, were derived from the OPLS-AA force fields, which was transformed from the MM3 force fields [21]. It was shown in our recent work that the obtained parameters for Pra work reasonably well in predicting backbone dihedral angles. The simulations for NMA were carried out in a periodic cubic box with side length set to 28 Å. There were one NMA and 661 TIP3P D_2O molecules [22]. The simulation boxes for PPTP and PATP were quite similar, both have side length set to 30 Å. Inside the box, it has one PPTP molecule dissolved in 799 TIP3P D_2O molecules, or one PATP molecule dissolved in 800 TIP3P D_2O molecules. The non-bonded cutoff was set to 12 Å, and the particle-mesh Ewald summation [23] was used for long range electrostatic interactions. The Langevin piston Nose-Hoover method [24, 25] was used for simulation in the isothermal-isobaric ensemble. Each of the molecular dynamics simulations started from an energy minimization process, followed by a heating process from 0 K to desired temperature over a 20 ps period respectively. The system was then allowed to equilibrate for 1 ns at the desired temperature. The MD simulations were finally performed for 1 ns at 298, 400, and 500 K for NMA, 298 and 500 K for PPTP and PATP, with a step of 2 fs. 5×10^5 evenly spaced snapshots were taken in each case to obtain instantaneous structural ensembles. High temperature MD simulations allow small peptides to explore more conformational space.

D. Instantaneous normal mode analysis and MM-map

The vibrational transition frequency of the amide-I mode of NMA at high temperature was calculated through the INM analysis using the VIBRAN module of CHARMM [26]. The instantaneous normal mode (INM) analysis was performed for the 500 thousand instantaneous structures from the 1-ns MD trajectory. Hessian matrix diagonalization at every instantaneous molecular configuration yielded the harmonic vibrational frequency for the amide-I mode. The distribution of the amide-I frequencies was obtained. Only the nuclear configurations of naked deuterated NMA molecule were considered for each snapshot and explicit solvent molecules were removed. No further structural opti-

DOI:10.1088/1674-0068/24/05/529-537

mization and energy minimized before the INM analysis because otherwise the influences of the explicit solvent molecules on NMA during the MD simulations would be eliminated.

E. MM-map frequency of the NMA amide-I mode

The method of parameterizing the MM-map has been given in detail in our recent work [11]. Briefly, we assume

$$\nu_{\rm INM} + \Delta\nu_{\rm INM} = \nu_0 + \Delta\nu_\varphi \tag{1}$$

where $\nu_{\rm INM}$ is the INM frequency, $\Delta\nu_{\rm INM}=\nu-\nu_{\rm INM}$ is the red shift from the INM frequency to the solution-phase fluctuating frequency of the amide-I, and $\nu_{\rm INM}$=1860 cm^{-1} was found and thus $\Delta\nu_{\rm INM}$=−57.0 cm^{-1} was determined for NMA at 298 K [11], ν_0 is the gas phase experimental frequency (ν_0=1717 cm^{-1}) of NMA [27], $\Delta\nu_\varphi$ is the electrostatic potential caused red shift of the gas-phase frequency to ν. Thus we have

$$\nu = \nu_0 + \Delta\nu_\varphi \tag{2}$$

Rewrite $\Delta\nu_\varphi$ in terms of the electrostatic potential, we have

$$\nu = \nu_0 + \sum_i f_i\varphi_i \tag{3}$$

here f_i and φ_i are coefficients and electrostatic potentials exerted on four sites of NMA (Fig.1): C(=O), O(=C), N, and D(−N). The potential due to peptide itself and solvent molecules is obtained by

$$\varphi_i = \frac{1}{4\pi\varepsilon_0}\sum_k \frac{q_k}{r_{i,k}} \tag{4}$$

where q_k is the atomic partial charge of the kth atom of the system, *i.e.*, water molecules and the two CH_3 groups of NMA. Here the two methyl groups were treated as united atoms, with partial charges of three H atoms added to their C atoms. In Eq.(4), $r_{i,k}$ is the distance between the ith site of NMA and the kth atom of water molecules or the united atoms. The CHARMM atomic partial charges and TIP3P water charges ($q_{\rm O}$=−0.834 and $q_{\rm H}$=0.417) were used. By using Eq.(4) the electrostatic potentials coming from solvent molecules and NMA peripheral atoms were calculated for the four sites. In parameterization of the MM-map, Eqs. (1)−(4) were used. Multivariate least square fitting was carried out to obtain f_i at the four sites upon a sampling space containing ca. 200 evenly spaced instantaneous structures out of a 1 ns MD trajectory. Similar samplings were carried out for the MD simulations at three temperatures of 298, 400, and 500 K. The difference between the gas phase experimental frequency of the amide-I mode in NMA and that of the experimental value (1623 cm^{-1}) [28] is accounted by the electrostatic potentials exerted on the four sites.

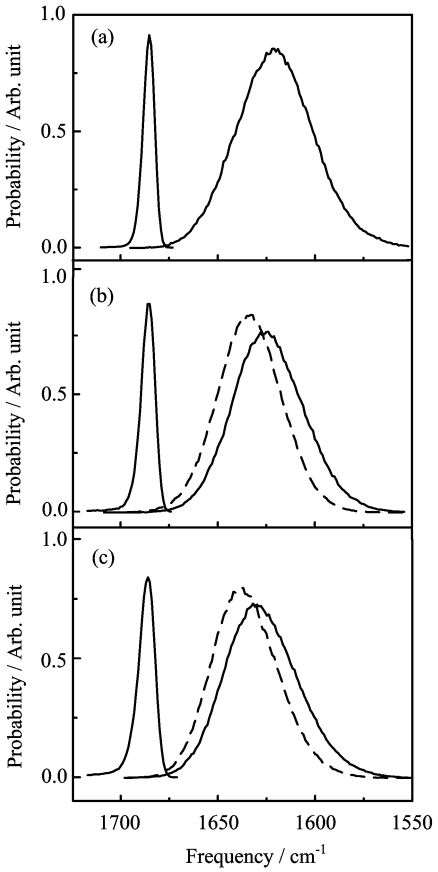

FIG. 2 Distribution of the INM frequencies (left solid curve), MM-map frequencies using the room-temperature parameters (right solid curve) and the MM-map frequencies using the MM-map parameters at each temperature (dashed curve) for the amide-I mode of NMA at 298 K (a), 400 K (b), and 500 K (c).

III. RESULTS AND DISCUSSION

A. INM and MM-map frequency distributions of NMA at the three temperatures

We first plot the amide-I normal mode frequency distributions computed using the INM analysis for NMA at 298, 400, and 500 K in Fig.2 (left solid curve). As temperature increases, the INM frequency distributions only blue-shift by less than 2 cm^{-1}, accompanied by a moderate band width change from 5.9 cm^{-1} to 9.8 cm^{-1} (full width half maximum, FWHM), indicating a temperature-insensitivity of the INM frequency. Obviously the band width of the INM frequency distribution is much narrower than that of the experimentally observed IR band (29 cm^{-1}) as shown below. Since the INM frequency distribution is unrealistic, a solution-phase frequency map is needed.

However, the amide-I frequencies obtained using the MM-map at 298 K which was constructed before, whose parameters were listed in Table I, exhibit a clear

DOI:10.1088/1674-0068/24/05/529-537

TABLE I MM-map parameters (in cm^{-1}/V) for the 0-1 transition frequency of the amide-I mode of NMA in D_2O at different temperatures T.

T/K	f_C	f_O	f_N	f_D
298	79.441	−19.880	−121.026	54.817
400	77.553	−24.776	−101.904	41.426
500	74.575	−21.787	−106.101	46.716

temperature-sensitivity. The map parameters were defined in Eq.(3). The f_C, f_O, f_N, and f_D are coefficients for the electrostatic potentials caused by the peptide and solvent molecules. From the absolute magnitude of the coefficient, it is concluded that the amide-I mode solution frequency is most sensitive to the N-position and the least sensitive to the O-position. Such sensitivities remain similar for the three maps developed respectively at three temperatures. To obtain the amide-I frequencies, the 298-K map was applied to 298, 400, and 500 K MD simulations of NMA (Fig.2, right solid curves). The peak positions and widths of the INM and MM-map frequency distributions were summarized in Table II.

We now compare the performance of the each map. For the results obtained using the 298-K map, at 298 K, a red shift of ca. 62 cm^{-1} is seen from the INM frequency to the MM frequency. As the temperature changes from 298 K to 500 K, the most probable MM-frequency blue shifts from 1622.6 cm^{-1} to 1628.0 cm^{-1}, accompanied by a band width decrease from 45.7 cm^{-1} to 36.2 cm^{-1}. This is mainly due to the change in NMA-solvent hydrogen-bonding interactions: statistically less solvent molecules appear in the neighborhood of NMA at high temperature. This is verified by the MD simulations carried out at each temperature. Figure 3 shows the radial distribution functions $g(r)$ for selective pairs of atoms in the solvated NMA at different temperatures. The integrated areas of $g(r)$ for the first peak, representing the density of water in the first hydration layer, are found to decrease as the MD temperature increases (Fig.3). Thus, the broadening and red shift of the most probable frequency from the INM picture to the MM-map picture is an indicator that the MM frequency can sense the electrostatic influences of the solvent exert on peptide. Such influences causes homogeneous and inhomogeneous line broadenings in the amide-I absorption band, while the INM frequency distribution as shown previously [11] does not contain inhomogeneous contribution.

A set of MM-map parameters was also developed for the solvated NMA at 400 and 500 K respectively (Table I). It is found that the coefficient f_C, f_O, f_N, and f_D show different temperature dependences. We were unable to find a reasonable explanation for the temperature dependences. However, we examined the performances of the high-temperatures maps. The 400-K and 500-K map were applied to the MD simulations at corresponding temperatures respectively, and resultant amide-I frequency distributions were shown in Fig.2 (dashed line) and Table II (in parenthesis). The MM-frequency peak position obtained using the 400-K map applied on the 400 K MD trajectories (Fig.2(b) dashed line) is more blue-shifted than that obtained using the 298-K map applied on the 400 K MD trajectories (Fig.2(b), right solid line). Similar case is seen in Fig.2(c). However, as seen in the next section, these frequency peak positions were actually over shifted and did not agree with the FTIR absorption maxima. Instead, we found the 298-K frequency map worked for NMA at both 298 and 500 K. Thus in the following text the room-temperature MM-map shall be used for peptides in this work unless otherwise stated.

TABLE II The temperature-dependent INM frequency and MM-map frequency distributions of NMA (the frequency peak position ν_{max} and FWHM Γ). The MM-map results are obtained using the 298-K map except those in parenthesis, which are obtained using the 400-K and 500-K map respectively.

T/K	INM		MM-map	
	ν_{max}/cm^{-1}	Γ/cm^{-1}	ν_{max}/cm^{-1}	Γ/cm^{-1}
298	1684.8	5.9	1622.6	45.7
400	1685.4	8.0	1625.5 (1634.2)	38.5 (36.7)
500	1686.0	9.8	1628.0 (1638.9)	36.2 (34.8)

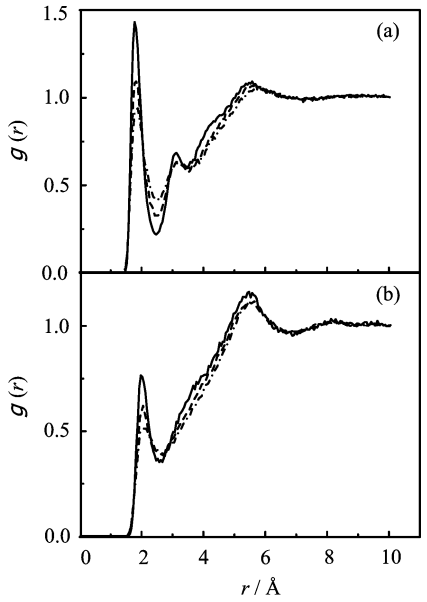

FIG. 3 Radial distribution functions for selective pairs of atoms in the solvated NMA at different temperatures. (a) $O(=C)\cdots H(H_2O)$ and (b) $H(-N)\cdots O(H_2O)$. Solid line: ones at 298 K, dashed line: ones at 400 K, dot-dashed lines: ones at 500 K and the integrated areas of the first peak of the three curves are 0.76, 0.72 and 0.70 in (a), and 0.47, 0.45 and 0.43 in (b), respectively.

DOI:10.1088/1674-0068/24/05/529-537

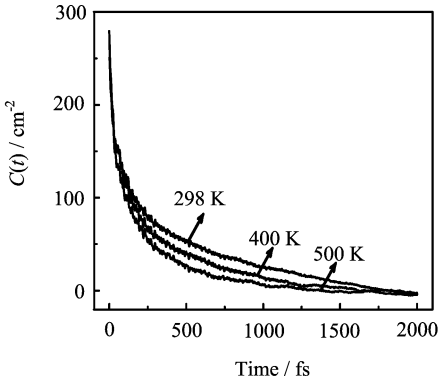

FIG. 4 Temperature dependence of the frequency TCFs for the amide-I mode of NMA.

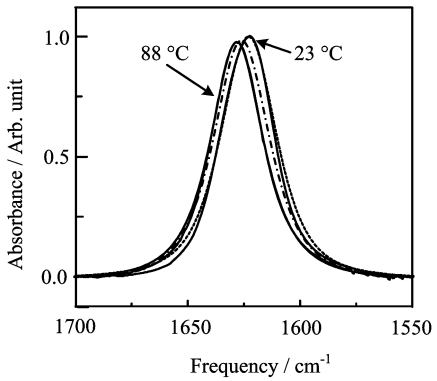

FIG. 5 The amide-I FT IR spectra of NMA solvated in D_2O at 23 and 88 °C (solid) and the simulated IR spectra (dashed). The simulated spectrum at 400 K was also given (dot-dashed).

B. Amide-I linear IR spectral simulation for NMA

From the 1 ns frequency trajectories of NMA obtained using the MM-map shown in Fig.2, the frequency TCF was calculated

$$C(t) = \langle \delta\nu(t)\delta\nu(0)\rangle \tag{5}$$

where $\delta\nu(t)=\nu(t)-\langle\nu\rangle$ and $\langle\nu\rangle$ is the average frequency. This is the two-point time-correlation function, which is a simple well-known function used to describe the fluctuating frequency of a specific vibrational mode caused by solute and its chemical surroundings in the solution phase. Thus the frequency TCF can be used to characterize the dynamics of the solute and solvent as well [14]. The frequency TCF is a quantity that can be derived from ultrafast vibrational spectroscopy.

The resulting frequency TCFs for the amide-I mode in NMA at the three temperatures were shown in Fig.4. It can be seen that the three curves are apparently different. A two-component exponential function is used to fit the frequency TCF:

$$C(t) = \sum_{i=1}^{2} \Delta_i^2 \exp\left(-t/\tau_i\right) \tag{6}$$

The fitting parameters obtained at the three temperatures were listed in Table III. Both the fast and slow component have their time constants (τ_1 and τ_2) becoming significantly smaller as temperature increases; while their relative amplitudes (Δ_1 and Δ_2) both only increase slightly, but the relative weights only change insignificantly.

Further, from Eq.(6) the line shape function $g(t)$ was obtained with the aid of the cumulant expansion method [29−31]:

$$g(t) = \int_0^t \mathrm{d}t_1 \int_0^{t_1} \langle \delta\nu\left(t_2\right) \delta\nu\left(0\right)\rangle \, \mathrm{d}t_2 \tag{7}$$

The linear IR absorption spectrum was then obtained

$$I(\nu) = \int_{-\infty}^{+\infty} \exp\left[-i(\nu - \langle\nu\rangle)t - g(t) - \frac{t}{2T_1}\right]\mathrm{d}t \tag{8}$$

TABLE III The frequency TCF fitting parameters Δ_1 (in cm^{-1}), Δ_2 (in cm^{-1}), τ_1 (in fs) and τ_2 (in fs) of the amide-I mode in NMA at different temperatures T. The peak positions (ν_{max}, in cm^{-1}) and the line widths (Γ, in cm^{-1}) of the simulated linear IR spectra were also listed.

T/K	Δ_1	τ_1	Δ_2	τ_2	ν_{max}	Γ
298 [11]	12.3	45.6	11.0	676.0	1622.6	29.5
400	12.6	42.8	12.0	459.8	1625.5	29.6
500	12.9	35.4	12.4	322.6	1628.0	27.6

Here T_1 is the lifetime of the first vibrational excited state of the amide-I mode of NMA, which was set to 0.45 ps [32]. The calculated linear IR spectra of the amide-I mode of NMA at the three temperatures were given in Fig.5. Experimental IR spectra at 23 and 88 °C were also given for comparison. At 298 K, reasonable agreement of both peak position and FWHM was found between the simulated IR spectrum and experiment result obtained at 23 °C. At 500 K, one sees that the simulated IR spectrum also shows a reasonable agreement with the 88 °C FTIR result. The simulated linear IR spectrum at 400 K was also shown in Fig.5 (dot-dashed line), which has its peak position and line width nicely put in between the 298 and 500 K simulation results. These results indicate that our MM-map can reasonably reproduce the temperature dependent experimental IR spectra of the amide-I band of NMA. In addition, we also found that when the room-temperature frequency map was applied on the MD simulations at below 500 K temperature, the FTIR spectrum at 88 °C can not be reproduced. Thus we believe the MD simulations at 500 K corresponds to IR experiment at 88 °C as far as the IR spectrum is concerned in this work.

DOI:10.1088/1674-0068/24/05/529-537

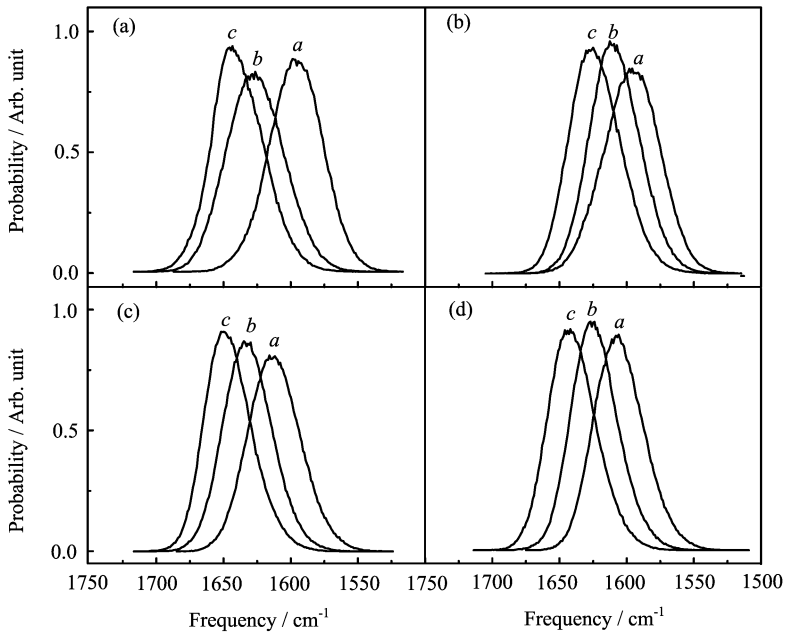

FIG. 6 Static distributions of the amide-I local mode transition frequencies of three amide units (a, b, and c) in PPTP and PATP at two temperatures. (a) PPTP at 298 K, (b) PATP at 298 K, (c) PPTP at 500 K, and (d) PATP at 500 K.

C. Application of the MM-map on PPTP and PATP

Using the MM-map, we computed the three amide-I local mode frequencies in the D_2O-solvated PPTP and PATP, based on the MD simulations at 298 and 500 K. The static distributions of the amide-I transition frequencies were shown in Fig.6. It appears that the local mode transition frequency of the amide unit-c is mainly at the high-frequency side, and that of the amide unit-a is mainly at the low-frequency side both in PPTP and PATP at room and high temperatures. In PPTP at room temperature, the frequency separation between the transition frequencies of the amide unit-c and unit-b is greater than the one between the amide unit-a and unit-b. In PATP at room temperature, the frequency separation is similar to each other. As temperature rises, one can see that the frequency of amide unit-c displays a blue-shift of about 10 cm^{-1} and each of the other two amide units displays a blue-shift of about 5 cm^{-1} in PPTP, suggesting that the chemical environment of the amide unit-c changes more significantly than those of the other two amide units as temperature rises. For PATP at high temperature, all the three amide-I transition frequencies display blue-shifts about 10−15 cm^{-1} comparing with those at room temperature. Further, one can see that in Fig.6, for PPTP, the local mode frequency distributions of three amide units show similar FWHM at 298 K, however, with different ν_{max}. At 500 K, the bandwidths become narrow and peak positions are blue shifted and become somewhat closer to one another. The situations of PATP are quite similar.

The frequency TCFs of the three amide-I local modes in PPTP and PATP were shown in Fig.7. The TCF bi-exponential fitting parameters were shown in Table IV. In Fig.7, the three TCFs for the amide unit-a, unit-b, and unit-c in each case are different in both the fast and slow components. The difference between unit-a, unit-b, and unit-c shown in Fig.6 and Fig.7 can be mainly attributed tothe peptide-solvent interactions, in particular the hydrogen-bonding interactions. For ex-

TABLE IV The frequency TCF fitting parameters Δ_1 (in cm^{-1}), Δ_2 (in cm^{-1}), τ_1 (in fs) and τ_2 (in fs) of each amide-I mode in PPTP and PATP, the static distribution of the three amide-I local mode frequencies (ν_{max}, in cm^{-1}) and the simulated IR absorption line width (Γ, in cm^{-1}) at the two temperatures.

Tripeptide	Δ_1	τ_1	Δ_2	τ_2	ν_{max}	Γ
			298 K			
PPTP-a	10.09	37.6	10.27	628.7	1598.6	26.9
PPTP-b	9.03	43.0	10.51	823.6	1628.5	28.4
PPTP-c	9.07	45.0	11.29	720.4	1645.7	29.6
PATP-a	10.05	50.2	8.87	690.8	1598.2	24.8
PATP-b	9.68	37.2	9.64	664.0	1612.2	25.7
PATP-c	9.92	46.9	9.74	733.1	1628.3	26.7
			500 K			
PPTP-a	12.08	28.6	11.56	391.2	1609.2	26.9
PPTP-b	11.83	30.3	10.77	565.6	1627.6	27.5
PPTP-c	12.48	35.4	11.00	433.0	1645.6	26.9
PATP-a	12.42	29.1	11.06	391.0	1608.6	26.1
PATP-b	11.86	30.5	11.34	540.1	1626.8	28.5
PATP-c	12.04	33.2	10.93	392.1	1643.6	26.0

DOI:10.1088/1674-0068/24/05/529-537

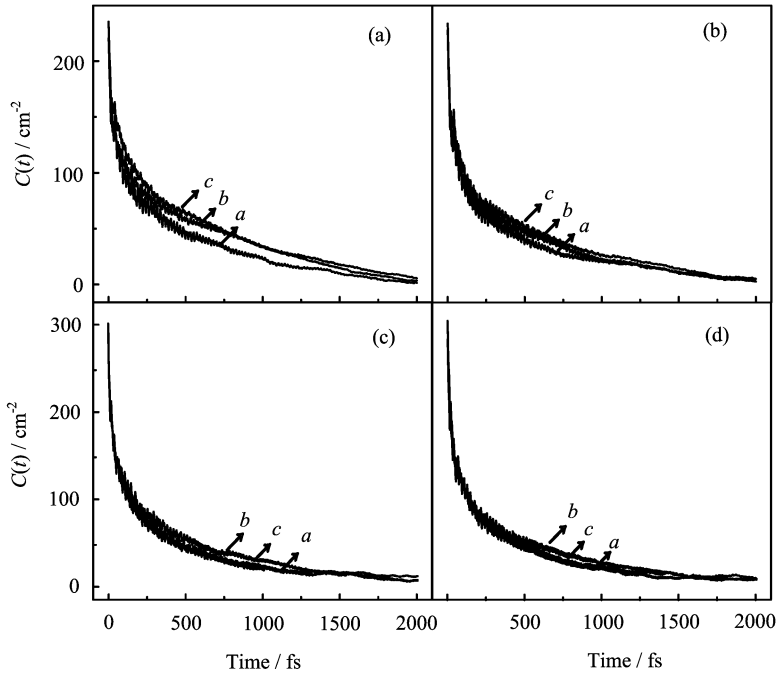

FIG. 7 Frequency TCFs for the three amide-I local modes (amide units *a*, *b*, and *c*) of PPTP and PATP at two temperatures of 298 and 500 K. (a) PPTP at 298 K, (b) PATP at 298 K, (c) PPTP at 500 K, and (d) PATP at 500 K.

ample, statistically the C=O and N−H groups of the amide-*a* are less blocked by the propargyl and methyl side chain groups in PPTP and PATP, and thus the amide-*a* shows the largest red shift in its amide-I local mode frequency. It also shows a generally more different dynamics TCF than unit-*b* and unit-*c*. The results of Fig.6 and Fig.7 reflect that these three amide units are in somewhat different chemical environments.

To simulate the amide-I linear IR spectra of PPTP and PATP, a fluctuating Hamiltonian protocol was used [17]. Briefly, the *k*th normal mode frequency TCF can be approximated by a linear combination of the local mode TCFs:

$$C_k(t) = \sum_i V_{ik}^{-4} \langle \delta\nu_i(t)\, \delta\nu_i(0) \rangle \qquad (9)$$

where V is the eigenvector of an averaged local mode Hamiltonian: $V^{-1}HV{=}\Lambda$, and Λ is the eigenvalue. The Hamiltonian is [3×3] in dimension, and is composed of the diagonal elements, which are the MM-map computed averaged zeroth-order frequencies (Fig.6); and off-diagonal elements, which are the averaged vibrational couplings (not shown), computed using a transition charge coupling scheme [33, 34]. Five hundred thousand MD structures were used to compute the zeroth-order frequencies and couplings. The simulated IR spectra were obtained using Eq.(7) and Eq.(8), with the lifetime of the first vibrational excited state of the amide-I mode in peptides, T_1, set to 0.8 ps [32]. The transition dipole strength in the normal mode picture was taken into account to simulate the linear IR spectra of three eigenmodes using Eq.(8).

TABLE V Peak position (ν, in cm^{-1}) and line width (Γ, in cm^{-1}) of the FTIR and simulated IR spectra in the amide-I region for PPTP and PATP at two temperatures T.

T/K	Tripeptide	FTIR		Simulated IR		$\nu-\nu'$
		ν	Γ	ν'	Γ'	
298	PPTP	1651.1	53.3	1624.7	51.2	26.4
	PATP	1644.3	49.6	1619.4	49.0	24.9
500	PPTP	1655.9	51.2	1633.8	52.9	22.1
	PATP	1647.7	48.0	1627.5	49.2	20.2

The simulated IR spectra in the amide-I region for PPTP and PATP at 298 and 500 K were shown in Fig.8. The experimental FTIR spectra of PPTP and PATP at room and high temperatures were also shown for comparison. The peak positions and line widths of the experimental FTIR spectra and those of the simulated IR spectra at the two temperatures are listed in Table V.

As can be seen in Fig.8, a general agreement in IR band features between experiment and simulation at the two temperatures is obtained for both PPTP and PATP. Also as shown in Table V, the simulated line widths at the two temperatures well reproduce the experimental results for both PPTP and PATP. A blue shift of the absorption maximum from low temperature to high temperature observed in experiment is also reproduced in simulations. A slightly more blue shift is predicted at high temperature, as can be seen from the

DOI:10.1088/1674-0068/24/05/529-537

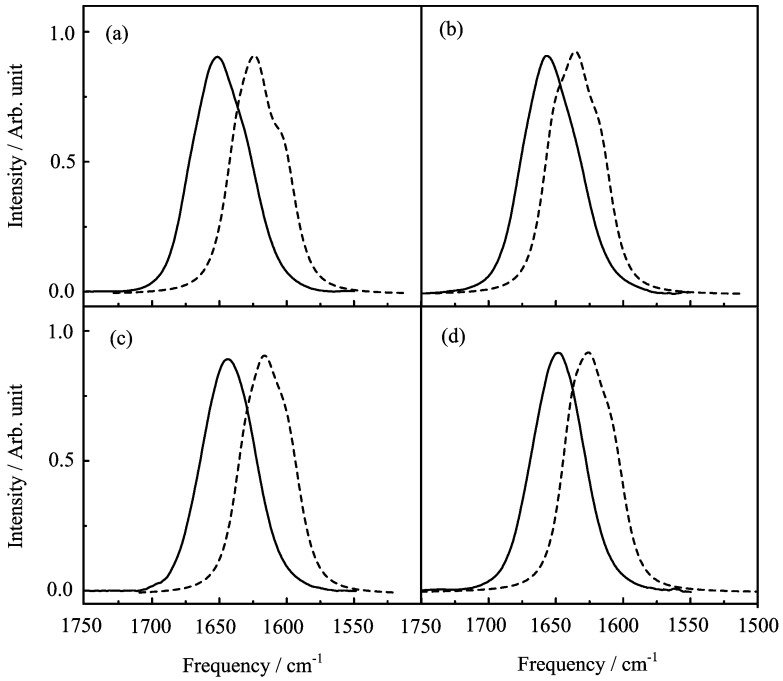

FIG. 8 FTIR (solid) and simulated IR (dashed) spectra of the amide-I modes of PPTP and PATP at different temperatures. (a) PPTP at 25.5 °C, (b) PPTP at 78.5 °C, (c) PATP at 24.0 °C, and (d) PATP at 79.2 °C.

$\nu-\nu'$ values listed in Table V. However, there is a general disagreement between the simulated peak positions and the IR experiment in all cases. This could be due to the inaccuracy of our MM frequency map so as to cause the local mode frequencies of the unit-*a*, unit-*b*, and unit-*c* to be over red-shifted. With those corrections taken into account, the agreement between the computations and experiments would be better. A better MM-map for the amide-I frequency is under construction in order to have an improved performance. In this new map, the two methyl groups in NMA shall be better treated, and the side chain effect shall be taken into account in parameterizing the map.

IV. CONCLUSION

In this work we have demonstrated that the MM-map for the amide-I local mode frequencies of peptides can be constructed at any given temperature, based on classical MD simulations. Temperature-dependent peptide conformational dynamics and solvent dynamics and their influences on the amide-I frequency are explicitly taken into account in terms of electrostatic interactions. By evaluating on a four-site basis on peptide backbone, such influences were proven to be quite successful, as exampled in NMA. Further, even though the frequency map was developed on the basis of molecular mechanics force fields, the method presented here can be extended to, for example, *ab initio* MD simulations.

Our results demonstrate that the MM-map based approach can be used to obtain the local mode frequencies and their distributions of peptides being at the thermally equilibrated states. For the single amide unit, a reasonable agreement between the simulated IR spectra and experimental results was observed at both room temperature and high temperature (up to 88 °C). Using the 298-K frequency map, local mode frequencies of two tripeptides containing natural and unnatural amino acid residues as a function of temperature can be examined in a straightforward way. It is well known that the amide-I band usually undergoes a thermal melting transition at ca. 75−80 °C, which is associated with the unfolding process of peptides and proteins. It is of great importance to get more insight into the structures and structural distributions of peptides and proteins in this temperature region. Our results suggest that the peptide conformational dynamics extracted from a 500-K MD simulations using the CHARMM force field roughly corresponds to that in aqueous solutions at 80 °C or so, as far as the IR signature of the amide-I mode is concerned. However, the simulated linear IR spectra of the two tripeptides, even though having a band structure in agreement with experimental IR spectra at both temperatures tested here, showed difference in peak position. This is mainly due to that the local mode frequencies of the three amide-I modes are somewhat over red-shifted. Such deviations are expected to diminish in new frequency maps that better take into account the electrostatic interactions involving peptide side chains and solvent molecules.

DOI:10.1088/1674-0068/24/05/529-537

V. ACKNOWLEDGMENTS

This work was supported by the National Natural Science Foundation of China (No.30870591), the National Basic Research Program of China (No.2007CB815205), and the Chinese Academy of Sciences (Hundred Talent Fund). Chen Han thanks Dr. Kai-cong Cai for helpful discussions.

[1] A. Remorino, I. V. Korendovych, Y. Wu, W. F. DeGrado, and R. M. Hochstrasser, Science **332**, 1206 (2011).
[2] D. B. Strasfeld, Y. L. Ling, R. Gupta, D. P. Raleigh, and M. T. Zanni, J. Phys. Chem. B **113**, 15679 (2009).
[3] C. Kolano, J. Helbing, M. Kozinski, W. Sander, and P. Hamm, Nature **444**, 469 (2006).
[4] J. Wang, W. Zhuang, S. Mukamel, and R. Hochstrasser, J. Phys. Chem. B **112**, 5930 (2008).
[5] C. Y. Huang, Z. Getahun, Y. Zhu, J. W. Klemke, W. F. DeGrado, and F. Gai, Proc. Natl. Acad. Sci. USA **99**, 2788 (2002).
[6] H. Maekawa, C. Toniolo, Q. B. Broxterman, and N. H. Ge, J. Phys. Chem. B **111**, 3222 (2007).
[7] H. S. Chung, M. Khalil, A. W. Smith, Z. Ganim, and A. Tokmakoff, Proc. Natl. Acad. Sci. USA **102**, 612 (2005).
[8] L. Wang, C. T. Middleton, M. T. Zanni, and J. L. Skinner, J. Phys. Chem. B **115**, 3713 (2011).
[9] H. Maekawa and N. H. Ge, J. Phys. Chem. B **114**, 1434 (2010).
[10] Y. S. Lin, J. M. Shorb, P. Mukherjee, M. T. Zanni, and J. L. Skinner, J. Phys. Chem. B **113**, 592 (2009).
[11] K. Cai, C. Han, and J. Wang, Phys. Chem. Chem. Phys. **11**, 9149 (2009).
[12] T. L. Jansen and J. Knoester, J. Chem. Phys. **124**, 044502/1 (2006).
[13] T. Hayashi, W. Zhuang, and S. Mukamel, J. Phys. Chem. A **109**, 9747 (2005).
[14] J. R. Schmidt, S. A. Corcelli, and J. L. Skinner, J. Chem. Phys. **121**, 8887 (2004).
[15] K. Kwac and M. Cho, J. Chem. Phys. **119**, 2247 (2003).
[16] P. Bour and T. A. Keiderling, J. Chem. Phys. **119**, 11253 (2003).
[17] S. Hahn, S. Ham, and M. Cho, J. Phys. Chem. B **109**, 11789 (2005).
[18] J. C. Phillips, R. Braun, W. Wang, J. Gumbart, E. Tajkhorshid, E. Villa, C. Chipot, R. D. Skeel, L. Kale, and K. Schulten, J. Comput. Chem. **26**, 1781 (2005).
[19] A. D. MacKerell, D. Bashford, M. Bellott, R. L. Dunbrack, J. D. Evanseck, M. J. Field, S. Fischer, J. Gao, H. Guo, S. Ha, D. Joseph-McCarthy, L. Kuchnir, K. Kuczera, F. T. K. Lau, C. Mattos, S. Michnick, T. Ngo, D. T. Nguyen, B. Prodhom, W. E. Reiher, B. Roux, M. Schlenkrich, J. C. Smith, R. Stote, J. Straub, M. Watanabe, J. Wiorkiewicz-Kuczera, D. Yin, and M. Karplus, J. Phys. Chem. B **102**, 3586 (1998).
[20] A. D. Mackerell, M. Feig, and C. L. Brooks, J. Comput. Chem. **25**, 1400 (2004).
[21] E. Goldstein, B. Ma, J. H. Lii, and N. L. Allinger, J. Phys. Org. Chem. **9**, 191 (1996).
[22] W. L. Jorgensen, J. Chandrasekhar, J. D. Madura, R. W. Impey, and M. L. Klein, J. Chem. Phys. **79**, 926 (1983).
[23] U. Essmann, L. Perera, M. L. Berkowitz, T. Darden, H. Lee, and L. G. Pedersen, J. Chem. Phys. **103**, 8577 (1995).
[24] S. E. Feller, Y. Zhang, R. W. Pastor, and B. R. Brooks, J. Chem. Phys. **103**, 4613 (1995).
[25] G. J. Martyna, D. J. Tobias, and M. L. Klein, J. Chem. Phys. **101**, 4177 (1994).
[26] B. R. Brooks, R. E. Bruccoleri, B. D. Olafson, D. J. States, S. Swaminathan, and M. Karplus, J. Comput. Chem. **4**, 187 (1983).
[27] L. C. Mayne and B. Hudson, J. Phys. Chem. **95**, 2962 (1991).
[28] M. T. Zanni, M. C. Asplund, and R. M. Hochstrasser, J. Chem. Phys. **114**, 4579 (2001).
[29] S. Mukamel, *Principles of Nonlinear Optical Spectroscopy, Oxford University*, New York: Oxford University Press, (1995).
[30] R. Kubo, Adv. Chem. Phys. **15**, 101 (1969).
[31] D. W. Oxtoby, J. Chem. Phys. **68**, 5528 (1978).
[32] P. Hamm, M. Lim, and R. M. Hochstrasser, J. Phys. Chem. B **102**, 6123 (1998).
[33] P. Hamm, M. Lim, W. F. DeGrado, and R. M. Hochstrasser, Proc. Natl. Acad. Sci. USA **96**, 2036 (1999).
[34] J. Wang and R. M. Hochstrasser, Chem. Phys. **297**, 195 (2004).

DOI:10.1088/1674-0068/24/05/529-537